Mechanistic Investigation of Peptidylglycine α-Hydroxylating Monooxygenase via Intrinsic Tryptophan Fluorescence and Mutagenesis†

Joseph Bell,‡ Rajaâ El Meskini, Darlene D'Amato, Richard E. Mains, and Betty A. Eipper*

Department of Neuroscience, The University of Connecticut Health Center, Farmington, Connecticut 06030

Received February 12, 2003; Revised Manuscript Received April 28, 2003

ABSTRACT: The biosynthesis of the majority of biologically active peptides ends with an obligatory α-amidation step that is catalyzed only by peptidylglycine α-hydroxylating monooxygenase (PHM). The utility of two mechanisms proposed for this copper- and ascorbate-dependent monooxygenase was examined using site-directed mutagenesis and intrinsic tryptophan fluorescence. Retention of full activity by PHMccGln^{170}Ala and -Asn eliminates a critical role for Gln^{170} in a substrate-mediated electron transfer pathway. The 20-fold reduction in V_{max} observed for PHMccGln^{170}Glu and -Leu is consistent with a key role for conformational changes in this region. Mutation of Tyr^{79}, situated near Cu_A, to Trp reduced V_{max} 200-fold. Measurement of changes in intrinsic fluorescence allowed determination of a K_d for copper (0.06 μM) and for a peptidylglycine substrate, Phe-Gly-Phe-Gly (0.8 μM). Although the peptidylglycine substrate bound more tightly at pH 7.0 than at pH 5.5, V_{max} decreased 25-fold at neutral pH. Total quenching of the signal from Trp^{79} in apoPHMccTyr^{79}Trp along with its greatly reduced V_{max} defines a critical role for Cu_A in the rate-limiting step of the reaction. Taking into account our data and the results of kinetic, spectroscopic, and crystallographic studies, we propose a mechanism in which substrate-mediated activation of molecular oxygen binding at Cu_A completes a pathway for electron transfer from Cu_B.

Copper-containing proteins are critical for a variety of cellular functions from electron transfer to dioxygen activation. Copper-dependent monooxygenases facilitate the activation of molecular oxygen and the incorporation of oxygen into product (*1*−*5*). Peptidylglycine α-hydroxylating monooxygenase (PHM,[1] EC 1.14.17.3) is a copper- and ascorbate-dependent monooxygenase that catalyzes the stereospecific α-hydroxylation of glycine-extended neuronal and endocrine peptide precursors, leading to the formation of α-amidated products and glyoxylate (Figure 1). PHM is a member of the family of structurally related copper- and ascorbate-dependent monooxygenases that includes dopamine β-monooxygenase and monooxygenase X (*4*). Despite kinetic studies, site-directed mutagenesis, crystallographic data, and EXAFS (extended X-ray absorption fine structure) studies, the mechanism through which PHM catalyzes peptide amidation remains unclear (*4*, *6*−*12*).

PHM and DBM function in the ascorbate-rich environment of the secretory pathway, making tight coupling of turnover to binding of peptidylglycine substrate and dopamine, respectively, a critical feature of the reaction. Although both PHM and DBM bind 2 mol of copper/mol of protein, neither EPR (electron paramagnetic resonance) nor EXAFS detected any coupling of the two copper ions (*8*, *12*−*14*). The presence of an 11 Å solvent-filled cleft separating the two copper ions bound to PHMcc (Cu_A, also termed Cu_H, and Cu_B, also termed Cu_M) undoubtedly contributes to this lack of coupling, raising the question of how the two reducing equivalents are used to catalyze the desired reaction (Figure 1).

Crystallographic, EXAFS, and kinetic data have provided different insights into possible reaction mechanisms. Largely on the basis of differences in the three-dimensional structures of the oxidized, substrate-bound catalytic core, and the reduced catalytic core of PHM [PHMcc, rPAM-1(42−356)], a substrate-mediated electron transfer pathway was proposed (*4*, *15*). More on the basis of Fourier transform infrared spectroscopy of carbon monooxide-bound PHM and EXAFS data, a superoxide-channeling mechanism was proposed (*6*, *7*, *10*). In the substrate-mediated electron transfer pathway, Gln^{170} plays a critical role in transferring reducing equivalents from Cu_A to the peptidylglycine substrate. Site-directed mutagenesis was used to explore the role of Gln^{170} in catalyzing peptide amidation. Gln^{170} was mutated to Asn or Glu, structurally conserved amino acids, to Leu, a hydrophobic amino acid of similar size, or to Ala, a small, nonpolar amino acid. The superoxide-channeling mechanism arose from the observation that peptidylglycine binding activates the binding of carbon monooxide to Cu_A (*6*). Tyr^{79}, located 4 Å from Cu_A, was postulated to assist in the channeling of superoxide, formed at Cu_A, toward Cu_B. To explore its role, Tyr^{79} was mutated to Phe or Trp. For the most diagnostic mutations, stable cell lines were generated so that mutant protein could be purified and analyzed.

† This work was supported by NIH Grant DK-32949.

* To whom correspondence should be addressed: Departments of Neuroscience, Biochemistry, and Physiology, University of Connecticut Health Center, 263 Farmington Ave., Farmington, CT 06030-3401. Phone: (860) 679-8898. Fax: (860) 679-1885. E-mail: eipper@uchc.edu.

‡ Current address: Department Ophthalmology, Columbia University, New York, NY 10027.

[1] Abbreviations: PHM, peptidylglycine α-hydroxylating monooxygenase; PAM, peptidylglycine α-amidating monooxygenase; PMSF, phenylmethanesulfonyl fluoride; EXAFS, extended X-ray absorption fine structure; FTIR, Fourier transform infrared spectroscopy; EPR, electron paramagnetic resonance.

10.1021/bi034247v CCC: $25.00
Published on Web 05/21/2003

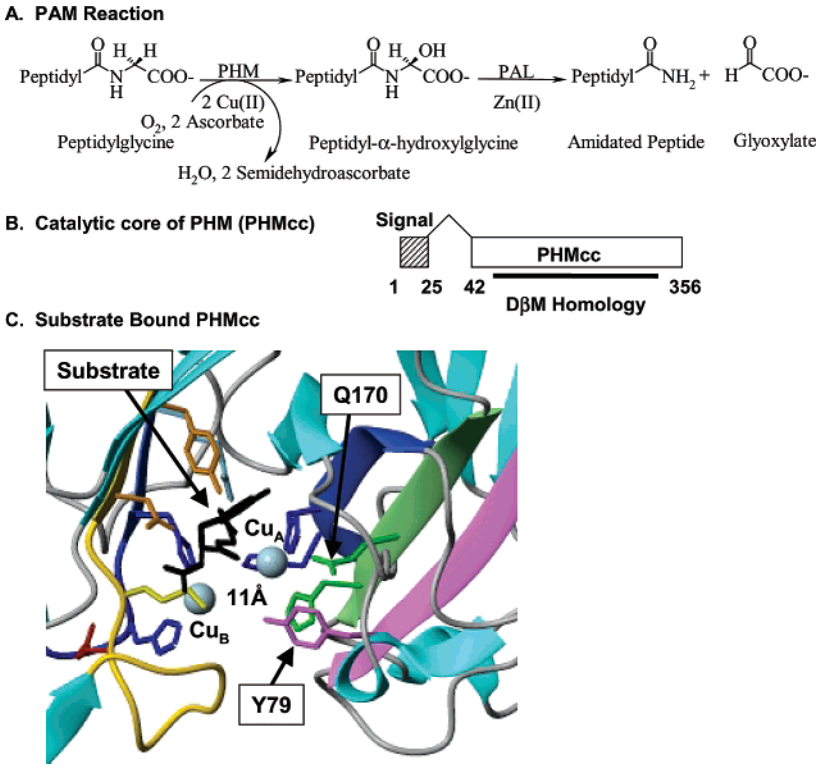

FIGURE 1: Peptide amidation and PHMcc. (A) PAM-catalyzed reactions. The reactions catalyzed by PHM and PAL are shown. (B) PHM catalytic core (PHMcc), with the region of homology between PHMcc and DβM indicated. (C) Active site of oxidized PHMcc, showing Cu_A and Cu_B separated by 11 Å. The bound [di-iodo]-acetyl-Tyr-Gly substrate is shown in black. Key residues are indicated, with the relevant β-strands and loops shown in a matching color: Tyr^{79}, β3, lavender; His^{107}, His^{108}, β5, dark blue; Gln^{170}, His^{172}, β9, light green; Arg^{240}, light blue; His^{242}, His^{244}, β14, following loop, dark blue; Glu^{313}, orange-red; Met^{314}, yellow; Asn^{316}, Tyr^{318}, β21, orange (*10*). The figure was created using MolMol.

Studies of PHM and PAM have largely been limited to analysis of the copper-bound enzyme. We employed intrinsic tryptophan fluorescence as a means of evaluating the effects of metal binding on protein structure. In addition, we used intrinsic tryptophan fluorescence to determine the K_d of the enzyme for its peptidylglycine substrate. PHMcc has only three Trp residues. By substituting a fourth Trp for Tyr^{79}, we hoped to generate a fluorescent marker that could monitor the active site. Our data suggest that neither the substrate-mediated electron transfer pathway nor the superoxide-channeling pathway provides an adequate description of the reaction catalyzed by PHMcc, leading us to suggest alternate possibilities.

MATERIALS AND METHODS

Construction and Analysis of PHMcc Mutants. The PHMccGln^{170} mutants (Gln^{170}Ala, Gln^{170}Glu, Gln^{170}Leu, and Gln^{170}Asn) and PHMccTyr^{79}Trp mutant were constructed by PCR-based mutagenesis of pBS.ΔproPHMcc356. Sense and antisense oligonucleotide primers encoding 21 bases upstream and downstream of the mutation were used. Primers used for each specific mutation were as follows: Gln^{170}Ala, 5′-GGAAGCAAATACTTCGTCCTTGCAGTTCACTATGGCGATATCAGTGC-3′; Gln^{170}Glu, 5′-GGAAGCAAATACTTCGTCCTTGAAGTTCACTATGGCGATATCAGTGC-3′; Gln^{170}Leu, 5′-GGAAGCAAATACTTCGTCCTTCTAGTTCACTATGGCGATATCAGTGC-3′; Gln^{170}Asn, 5′-GGAAGCAAATACTTCGTCCTTAACGTTCACTATGGCGATATCAGTGC-3′; and Tyr^{79}Trp, 5′-ACACCTAAAGAGTCTGACACATGGTTCTGCATGTCCATGCGTCT-3′. Changes from the wild-type sequence are underlined. Products generated by PCR were purified on agarose gels, digested with the appropriate restriction enzymes, and inserted into pBluescript as described previously (*16*). The coding region of each construct was sequenced in its entirety by the molecular Genomics Core Facilities at Johns Hopkins University School of Medicine (Baltimore, MD) or the University of Connecticut Health Center and inserted into the pEAK10 vector (*17*). The pCIS vector encoding ΔProPHM382s Tyr^{79}Phe was described previously (*10*).

Transient expression of PHMcc proteins was carried out in pEAK Rapid hEK293 cells using lipofectamine (Invitrogen, Gaithersburg, MD) (*17*). Cells were grown in DMEM-F12 supplemented with 10 mM HEPES, a penicillin/streptomycin mixture, and fetal bovine serum (Hyclone, Logan, UT). One day after transfection, transiently transfected cells were rinsed and fed with complete serum-free medium [CSFM; DMEM-F12 supplemented with HEPES, a penicillin/streptomycin mixture, and an insulin/selenium/transferrin mixture (Invitrogen)]; after 14−24 h, spent media and cells were harvested. Cells were extracted into 20 mM TES/NaOH, 10 mM mannitol, and 1% Triton X-100 (pH 7.4) containing protease inhibitors (*17*). To provide an accurate estimate of the amount of PHMcc protein in a sample of medium, aliquots of medium containing a range of PHMcc activity were subjected to SDS−PAGE and Western blot analysis using PHM polyclonal antibody JH 1761 (*18*). Following visualization of PHMcc protein by enhanced chemiluminescence (Pierce), films were scanned and the signals were quantified using NIH Scion Image.

Aliquots of spent medium yielding signals in the linear range of the film were used to calculate the amount of PHMcc protein present.

Purification of PHMcc Protein. Stably transfected CHO DG44 (*dhfr*-) cell lines secreting PHMcc (clone 6α) (*16*), PHMccGln^{170}Ala (clone B6), and PHMccTyr^{79}Trp (clone 7D7G) were established using pCIS vectors encoding each mutant protein and selected using αMEM (growth medium lacking nucleotides) supplemented with HEPES, a penicillin/streptomycin mixture, and 10% dialyzed fetal bovine serum. Clones were selected by screening spent medium for PHM activity and PHM protein (by Western blot). Highly producing clonal cell lines were grown in polylysine-coated 850 cm^2 roller bottles in growth medium (αMEM with dialyzed fetal calf serum) (*16*). Upon reaching confluence, the cells were rinsed in CSFM and fed with 200 mL of the same medium. Spent medium was collected daily and filtered through a 0.22 μm filter; phenylmethanesulfonyl fluoride (PMSF) (0.3 mg/mL) was added, and the medium was frozen until purification. For the first 2 or 3 weeks of collection, rollers were incubated in serum-containing medium over each weekend; established rollers continued to secrete PHMcc at slowly increasing levels for as long as 265 days (typically at least 100 days) before the cells sloughed off the surface of the roller bottle.

Protein purification was performed at 4 °C using a modification of published protocols (*15*, *16*, *19*). Proteins in 2 L of spent medium were precipitated by the addition of 0.611 g of $(NH_4)_2SO_4$/mL followed by centrifugation for 60 min at 6000 rpm. Pellets were suspended in 4−8 mL of MilliQ water, and two or three pellets were pooled. Particulate material was removed by centrifugation, and the supernatant was applied to a Sephadex G75-120 (Sigma) column (2 cm × 90 cm) equilibrated with 20 mM TES/NaOH and 0.5 M $(NH_4)_2SO_4$ (pH 7.0). Fractions containing PHMcc were identified by SDS−PAGE and pooled, and $(NH_4)_2SO_4$ was added to a final concentration of 1.5 M. The protein was further purified on a phenyl-Sepharose high-performance (Amersham Pharmacia Biotech) hydrophobic column (5 mL) equilibrated in 25 mM TES/NaOH and 1.5 M $(NH_4)_2SO_4$ (pH 7.0). Protein was eluted with a decreasing (from 1.5 to 0 M) $(NH_4)_2SO_4$ concentration gradient in 25 mM TES/NaOH buffer (pH 7.0). Fractions containing PHMcc were pooled and prepared for the MonoQ 5/5 (Amersham Pharmacia Biotech) column by buffer exchange in 25 mM TES/NaOH (pH 8) using a stirred flow cell (Amicon) fitted with a YM-30 (30 kDa molecular mass cutoff) membrane. The sample was then applied to a MonoQ column equilibrated in 25 mM TES/NaOH buffer (pH 8.0) and eluted with a gradient of increasing NaCl concentration (from 0 to 1 M) and decreasing pH (from pH 8 to 6). Fractions were analyzed on 4 to 15% SDS−PAGE gels and visualized by Coomassie staining or Western blotting. Fractions containing pure PHMcc were pooled and concentrated; enzyme activity was measured, and the protein concentration was determined by measuring A_{280} using the established extinction coefficient (*16*). Purification of the mutant PHMcc forms was unaltered from that for wild-type PHMcc. The extinction coefficient previously determined for PHMcc ($\epsilon = 1.29$ at 280 nm for 1 mg/mL) (*16*) was used for PHMccGln^{170}Ala; for PHMccTyr^{79}Trp, $\epsilon = 1.41$.

PHMcc Enzyme Assays. Aliquots of purified enzyme, spent medium, and cell extract were assayed as described previously (*16*) using 0.5 μM $CuSO_4$, 0.5 mM ascorbate, 0.5 μM acetyl-Tyr-Val-Gly, 0.1 mg/mL catalase, trace amounts of ^{125}I-labeled acetyl-Tyr-Val-Gly, and 150 mM NaMES (pH 5.5). Acetyl-Tyr-Val-Gly kinetic parameters (K_m and V_{max}) were determined in the presence of 0.5 μM $CuSO_4$, 0.5 mM ascorbate, 0.1 mg/mL catalase, trace amounts of ^{125}I-labeled acetyl-Tyr-Val-Gly, 150 mM NaMES (pH 5.5), and 0.2−100 μM acetyl-Tyr-Val-Gly (*10*). Kinetic parameters for the peptide Phe-Gly-Phe-Gly (Bachem) were determined using 0.2−400 μM Phe-Gly-Phe-Gly. Assays were performed in duplicate, and peptide controls were performed in the absence of PHMcc protein. For reactions that included Phe-Gly-Phe-Gly, the 40 μL reaction was quenched with 5 μL of 10% trifluoroacetic acid (TFA) and then the mixture diluted with 500 μL of 0.1% TFA. The samples were centrifuged, and 500 μL of peptide control or enzyme reaction sample was subjected to HPLC analysis to separate substrate from product.

Intrinsic Tryptophan Fluorescence Analysis. Steady-state intrinsic tryptophan (Trp) fluorescence was recorded on a SPEX fluorimeter (Jobin Yvon Inc., Edison, NJ) using SPEXCO software. All Trp fluorescence emission spectroscopy was performed in 3 mL of 50 mM NaMES/NaOH and 50 mM NaCl (pH 6.0) at 25 °C. Emission spectra were corrected for the appropriate solvent blank, as well as for metal ions or substrate. An excitation wavelength of 295 nm was used in all experiments. Fluorescence emission intensity was recorded as a function of wavelength from 310 to 425 nm; wild-type and mutant PHMcc protein concentrations were typically 600−800 nM. Prior to measurement, PHMcc was treated with 10 mM EDTA at 4 °C for 60 min to remove adventitious metals, followed by four or five washes with metal-free, EDTA-free buffer (pH 6.0) in a 15 mL Millipore microconcentrator, followed by protein determination by BCA and A_{280}.

RP-HPLC Analysis. Reverse phase HPLC analyses were performed using Beckman Coulter System Gold software. Samples were separated on a C_{18} μBondapak column (Waters) equilibrated with 0.1% trifluoroacetic acid and eluted using a gradient to 80% CH_3CN and 0.1% trifluoroacetic acid. For all samples, 500 μL was injected using a Hamilton syringe and absorbance was monitored at 220 and 280 nm.

Copper and Peptide Substrate Binding Studies. Copper binding to the purified PHMcc proteins was assessed using a Millipore microconcentrator (30 kDa cutoff), with the copper in the retentate and flow-through subjected to analysis using an AA600 furnace spectrometer (Perkin-Elmer A Analyst 600). The amount of copper bound to the protein was calculated as the copper concentration in the retentate minus the flow-through, divided by the concentration of enzyme in the retentate. Acetyl-Tyr-Val-Gly and Phe-Gly-Phe-Gly were dissolved in 0.1 and 1% HCl, respectively. Final stock solutions were prepared by serial dilution in 50 mM MES/NaOH and 50 mM NaCl (pH 6.0). Substrate and enzyme (600 nM enzyme, 500 μL) were tumbled at 4 °C for 2 h and concentrated to 50 μL using a Millipore microconcentrator (30 kDa cutoff), and the retentate and flow-through were subjected to HPLC analyses as described above. Alternatively, microdialysis capsules (Spectra/Por

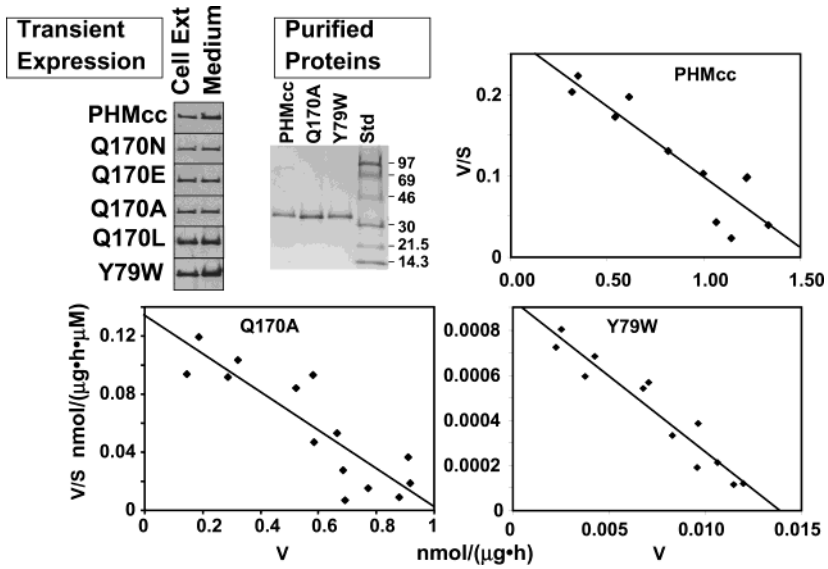

FIGURE 2: Analysis of PHMcc proteins transiently or stably expressed in hEK-293-derived pEAK Rapid cells. For Transient Expression, equal volumes of cell extracts and 24 h spent medium from cells expressing PHMcc or a PHMcc mutant were fractionated by SDS−PAGE, transferred, and visualized using a PHM antibody; the volume of medium that was analyzed was 6 times the volume of the cell extract, so equivalent signals for medium and cell extract mean that the content of the cell is secreted in approximately 4 h. The Western blot shows that mutation of Gln^{170} or Tyr^{79} did not affect the folding or secretion of PHMcc. For Purified Proteins, spent medium from stably transfected CHO cells was used to purify PHMcc, PHMccGln^{172}Ala, and PHMccTyr^{79}Trp; 2 μg of each PHMcc protein was fractionated by SDS−PAGE and visualized with Coomassie brilliant blue. For the Eadie−Hofstee plots, wild-type and mutant PHMcc were assayed in duplicate at pH 5.5 in the presence of ascorbate, copper, catalase, and various concentrations of Ac-Tyr-Val-Gly at 37 °C. The Michaelis constant (K_m) and V_{max} were determined by varying the tripeptide concentration over a 25-fold range. Data are representative of at least four experiments for each PHMcc protein.

Micro DispoDialyzer, 15 kDa cutoff; Spectrum, Laguna Hills, CA) were used to attempt to achieve equilibrium by dialysis, followed by HPLC analysis as described above.

RESULTS

Kinetic Analyses of Transiently Expressed Proteins

The monooxygenase activity of wild-type and mutant PHMcc proteins was assayed to determine the effect of mutating amino acids proposed to be critical to the substrate-mediated electron transfer mechanism (PHMccGln^{170}) or to the superoxide-channeling mechanism (PHMccTyr^{79}) (Figure 1). Since expression of active PHMcc in bacteria has not yet been accomplished, we screened the effects of these site-directed mutants by analyzing PHMcc secreted after transient expression in mammalian hEK-293 cells (Figure 2, Transient Expression). Stably transfected CHO cell lines were then established for the more diagnostic mutants. The activity of wild-type PHMcc and mutant enzyme was studied under various conditions (substrate and pH) to determine the effect of mutating these two active site residues. Gln^{170} was mutated to Asn or Glu, structurally related amino acids, to Leu, a hydrophobic amino acid of similar size, and to Ala, a much smaller, nonpolar residue. Tyr^{79}, which had previously been mutated to Phe (*10*), was also mutated to Trp to evaluate the effect of having a different large, hydrophobic residue with no hydroxyl group, as well as for use in Trp fluorescence studies.

Mammalian cells were transiently transfected with vectors encoding wild-type or mutant PHMcc, and the amount of PHM protein in cell extracts and medium was evaluated by Western blotting (Figure 2, Transient Expression). Each of the mutant proteins was secreted, and similar levels of protein were observed in cell extracts and medium for each of the mutants that were examined. Thus, none of these mutations of Gln^{170} or Tyr^{79} resulted in production of grossly malfolded or rapidly degraded enzyme. Since all of the mutant proteins were secreted, we used the spent medium to evaluate the effect of each mutation on the catalytic activity of PHM. We showed previously that accurate K_m and relative V_{max} values can be obtained by assaying secreted PHMcc without further purification (*10*).

Our initial assays, using a concentration of peptidylglycine substrate far below its K_m, revealed that all of the mutants retained some enzymatic activity. Substitution of Gln^{170} of PHMcc with Asn, Glu, Leu, or Ala resulted in Michaelis−Menten constants (K_m) comparable to that of wild-type PHMcc ($K_m = 11$ μM) (Table 1A). Substitution of Tyr^{79} of PHMcc with Trp gave a K_m value for Ac-Tyr-Val-Gly of 18 μM, not significantly different from that of wild-type PHMcc.

To estimate the effect of each mutation on V_{max}, aliquots of spent medium containing equal units of PHMcc activity (assayed with saturating amounts of substrate) were fractionated by SDS−PAGE and the amount of PHM protein was determined by Western blot analysis. Compared to the V_{max} of the wild-type enzyme, substitution of Gln^{170} with the negatively charged amino acid Glu or with the hydrophobic amino acid Leu resulted in a more than 10-fold reduction in V_{max}. Conversely, mutation of Gln^{170} to the structurally similar but smaller amino acid Asn or to the smaller and nonpolar amino acid Ala produced no difference between the mutant and wild-type V_{max}. Since replacement of Gln^{170} with Ala had been predicted from the crystal structure for elimination of the substrate-mediated electron transfer pathway, we generated a stable cell line producing this mutant protein. Substitution of Tyr^{79} with Trp reduced the relative V_{max} by approximately 50-fold. Since mutation of Tyr^{79} to Trp had a dramatic effect on V_{max} but did not totally eliminate

Table 1: Kinetic Constants

(A) Transiently Expressed PHMcc Proteins[a]

sample	K_m (μM)	relative V_{max} (pmol OD^{-1} h^{-1})
PHMcc	11 ± 5	1.00
PHMccGln^{170}Asn	9 ± 5	0.85
PHMccGln^{170}Glu	10 ± 5	0.07
PHMccGln^{170}Ala	18 ± 11	1.26
PHMccGln^{170}Leu	9 ± 5	0.05
PHMccTyr^{79}Trp	18 ± 10	0.02

(B) Purified PHMcc Proteins[b]

sample	pH	K_m (μM)	V_{max} (nmol μg^{-1} h^{-1})	k_{cat} (s^{-1})	k_{cat}/K_m (μM^{-1} s^{-1})
PHMcc	5.5	6.3 ± 1.4	1.5 ± 0.95	15.0	2.4
	7.0	1.2 ± 0.09	0.06 ± 0.01	0.53	0.2
PHMccGln^{170}Ala	5.5	6.5 ± 1.6	1.2 ± 0.6	14.0	2.2
	7.0	2.9 ± 1.0	0.07 ± 0.02	0.62	0.2
PHMccTyr^{79}Trp	5.5	9.8 ± 4.0	0.008 ± 0.004	0.09	0.009
	7.0	2.3 ± 1.4	0.0004 ± 0.0001	0.0035	0.0002

[a] PHM activity in medium samples from transiently transfected pEAK Rapid cells (Figure 2) was measured as described, and the amounts of the different PHMcc mutants were compared using an antibody to PHMcc. Data are representative of at least three experiments of this type for each PHMcc mutant. [b] Enzymes were assayed in the presence of Ac-Tyr-Val-Gly at pH 5.5 and 7.0 as described in Materials and Methods (mean ± standard deviation).

activity, we generated a stable cell line producing PHMcc-Tyr^{79}Trp.

Given that the protonation and/or deprotonation of residues at the active site may play an important part in the monooxygenase reaction, the activities of this set of mutant PHMcc proteins were measured as a function of pH (data not shown). When assayed between pH 4.0 and 7.0, the PHMccGln^{170} and -Tyr^{79} mutants exhibited broad maxima between pH 4.5 and 5.5 with very little activity above pH 6.5, much like wild-type PHMcc. Even substitution of Gln^{170} with Glu did not dramatically shift the pH profile of the reaction.

Kinetic Analyses of Purified PHMcc Mutants

Stably transfected CHO lines secreting PHMcc mutant proteins Gln^{170}Ala and Tyr^{79}Trp were created to allow production and purification of large quantities of protein for enzymatic, crystallographic, fluorescence, and other spectroscopic studies. The purification procedures for the two mutant proteins required no adjustment from the purification established for wild-type PHMcc, and the final preparations each consisted of a single major protein band (Figure 2, Purified Proteins). Initial velocity measurements were performed with purified wild-type PHMcc, PHMc-Gln^{170}Ala, and PHMccTyr^{79}Trp as a function of Ac-Tyr-Val-Gly substrate concentration at pH 5.5 and 7.0 (Figure 2 and Table 1B). Kinetic parameters (K_m and V_{max}) were determined by fitting the data to an Eadie−Hofstee plot (*20*, *21*).

At pH 5.5, the substitution of Gln^{170} with Ala had little effect on the Michaelis constant (K_m) or the rate of product formation (k_{cat}) when those values were compared to the wild-type values. On the other hand, while substitution of Tyr^{79} with Trp did not significantly alter K_m, it reduced the specific activity 200-fold compared to that of the wild-type enzyme. This finding suggests that Tyr^{79} normally plays a role in a rate-determining chemical step, e.g., substrate or dioxygen activation. The specificity constant (k_{cat}/K_m), which describes the relative affinity of the substrate for the enzyme (*20*), is almost 300-fold lower for PHMccTyr^{79}Trp than for wild-type PHMcc. In contrast, the specificity constants for PHMccGln^{172}Ala and wild-type PHMcc are identical.

Since copper coordination is controlled in large part by His residues in PHMcc, the effect of pH on enzymatic activity was examined (Table 1B). At pH 7.0, the K_m values of wild-type PHMcc, PHMccGln^{170}Ala, and PHMccTyr^{79}Trp for α-*N*-acetyl-Tyr-Val-Gly decreased 2−5-fold. Increasing the pH of the reaction mixture had a more dramatic effect on V_{max}. For all three enzymes, V_{max} decreased 20−30-fold when the pH was increased from 5.5 to 7.0 (Table 1B). As a result of the pH-dependent changes in both K_m and V_{max}, the specificity constants for all three enzymes decreased only ∼10-fold at pH 7.0 versus those at pH 5.5.

Steady-State Fluorescence Spectroscopy of Wild-Type PHMcc

Intrinsic fluorescence, using Trp as a reporter, can provide a sensitive and revealing measure of structure, solvent accessibility, and conformational change resulting from metal or substrate interaction (*22*, *23*). Wild-type PHMcc has three Trp residues (Trp^{124}, Trp^{141}, and Trp^{260}) (Figure 3A) (*4*). The side chain of Trp^{124}, which is conserved in all species of PHM, extends from the side of β-strand 6 facing away from Cu_A. Trp^{141}, part of the highly conserved hydrophobic sequence that forms β-strand 7, is 8.9 Å from Cu_A. Trp^{260}, located in β-strand 16, is 22.8 Å from Cu_B and is not conserved in all species of PHM.

Copper Binding to PHMcc. Although active PHMcc is known to require two bound coppers, a dissociation constant (K_D) for copper has not been measured. When our attempts to determine a dissociation constant for copper using equilibrium microdialysis devices and microconcentrators failed to provide clear data, we evaluated the effect of added copper on intrinsic Trp fluorescence emission intensity using steady-state fluorescence spectroscopy. An excitation wavelength of 295 nm was selected to optimize the signal from Trp, and fluorescence emission intensity was recorded as a function of wavelength from 310 to 425 nm. Prior to measurement, wild-type PHMcc was treated with EDTA to remove adventitious metal; atomic absorption spectroscopy revealed the presence of ≤0.25 mol of Cu/mol of protein following treatment. PHMcc exhibited maximal fluorescence intensity at 344 nm (Figure 3B), substantially below the λ_{max} for free Trp (358 nm) (*22*), indicating that the Trp residues in PHMcc are in a restricted, hydrophobic environment.

Fluorescence emission spectra for wild-type PHMcc were recorded following the addition of increasing amounts of copper, using a maximal copper concentration of 25 μM (Figure 3B). A biphasic decrease in fluorescence intensity was observed as the copper concentration was increased. The addition of similar concentrations of zinc or calcium had no effect on the fluorescence emission intensity of PHMcc (data not shown). To control for any direct effects of copper on Trp fluorescence not in the context of PHMcc, emission spectra were collected following the addition of copper to an equimolar solution of Trp; as the concentration of copper was increased above 1 μM, emission intensity decreased quite dramatically (not shown). For wild-type PHMcc (600 nM), loading with 2 μM copper yielded 1.6 ± 0.2 mol of Cu/mol

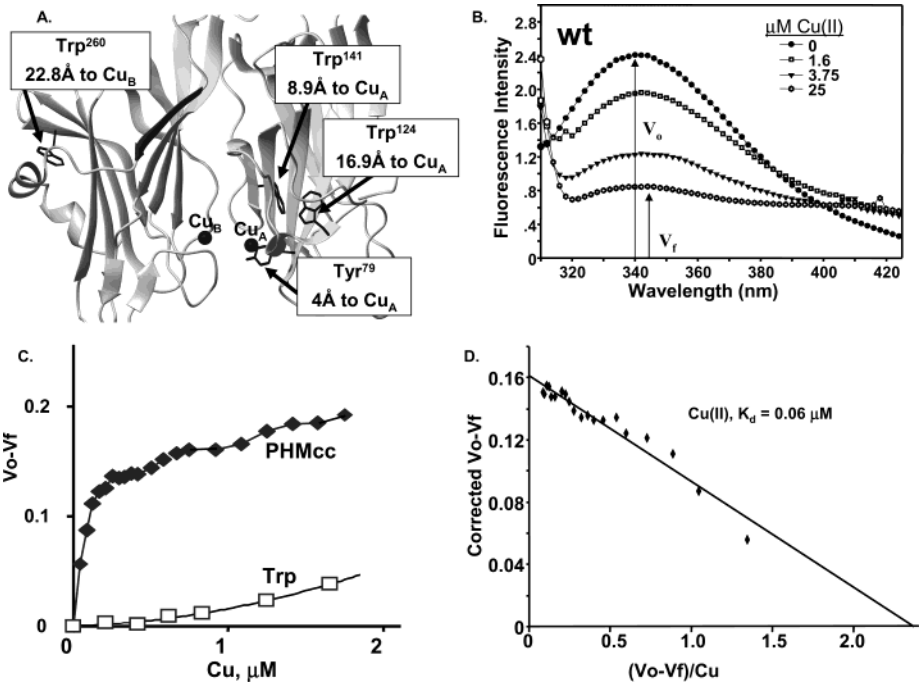

FIGURE 3: Effect of copper on tryptophan fluorescence of purified PHMcc. (A) The structure of oxidized PHMcc is shown with the three Trp residues indicated, along with the distance from each Trp to the nearest copper atom; Tyr^{79}, which was replaced with Trp in PHMcc-$Tyr^{79}Trp$, is also shown (*15*, *19*). (B) Fluorescence emission spectra of PHMcc (600 nM enzyme) show graded quenching with the addition of $Cu(NO_3)_2$. (C) Replotting the change in fluorescence at 344 nm as a function of Cu(II) concentration for PHMcc and for a solution of 1800 nM Trp. (D) Data for PHMcc over the 0−2 μM Cu(II) range are replotted from panel C with the contribution of free Trp subtracted. Data are representative of at least three experiments of this type.

of enzyme. Therefore, the response of PHMcc to copper concentrations of ≤ 2 μM was examined.

Changes in fluorescence emission intensity ($V_o - V_f$) at 344 nm were plotted as a function of copper concentration, revealing a dose-dependent effect that reached a plateau as copper levels rose above 0.5 μM (Figure 3C). After we had corrected for the direct effects of copper on free Trp [Figure 3C (□)], the effect of copper on the intrinsic Trp fluorescence of PHMcc was represented by a simple hyperbolic curve. An Eadie−Hofstee plot (Figure 3D) revealed a K_D of 0.06 μM for the interaction of copper with wild-type PHMcc. Collectively, these findings argue that the decrease in fluorescence emission intensity observed upon addition of sub-micromolar amounts of copper to PHMcc results from copper-dependent conformational changes in the tertiary structure of the enzyme. Since apoPHM cannot be examined by metal-dependent techniques such as EXAFS, this is the first indication that copper binding affects the conformation of PHM. Since Cu_B is further removed from any Trp residues than Cu_A, the measured affinity of PHMcc for copper, 0.06 μM, may reflect a greater contribution from Cu_A. The fact that incubation of the enzyme in 2 μM copper yields almost 2 mol of copper bound per mole of enzyme eliminates the possibility that the K_D for copper binding to Cu_B is substantially greater than 2 μM.

Steady-state fluorescence spectroscopy and copper titrations were carried out for PHMccGln^{170}Ala and PHMcc-$Tyr^{79}Trp$, yielding results indistinguishable from those of wild-type PHMcc (data not shown). The Tyr^{79} mutation, which had a dramatic effect on enzymatic activity, did not alter copper binding to the enzyme.

Ac-Tyr-Val-Gly Binding to PHMcc. No K_D for the binding of a peptidylglycine substrate to PHM has been assessed. We sought to extend the use of intrinsic Trp fluorescence to examine peptidylglycine substrate binding. On the basis of crystallographic data (*19*), peptidylglycine substrate binds near Cu_B, interacting with Arg^{240}, Phe^{318}, Asn^{316}, and Met^{314} (Figure 1C). The emission intensity of wild-type PHMcc devoid of copper was recorded following the addition of Ac-Tyr-Val-Gly (from 0 to 8 μM) (data not shown). No measurable differences in either emission intensity or λ_{max} were observed for the wild-type enzyme; similar results were seen in the absence of copper using the two purified mutant enzymes. Since the monooxygenase reaction requires copper bound to the enzyme, copper-loaded enzyme was tested next (Figure 4A). However, addition of the Ac-Tyr-Val-Gly substrate produced no significant change in Trp fluorescence using the copper-loaded enzyme. Similar results were obtained using the mutant PHMcc proteins (data not shown).

Phe-Gly-Phe-Gly (FGFG) as a Substrate for PHMcc. Since knowledge of the affinity with which PHMcc binds its peptidylglycine substrate is essential to understanding the kinetics of the reaction, we sought a different means of measuring this parameter. The lack of a shift in Trp fluorescence upon addition of peptide substrate (Figure 4A) could indicate that peptide binds weakly to the enzyme or that peptide binding fails to alter the enzyme in a way that affects Trp fluorescence. At concentrations above 10 μM, fluorescence emission from Ac-Tyr-Val-Gly obscures the signal from the enzyme. To evaluate peptidylglycine binding to PHMcc at higher peptide substrate concentrations, we explored the use of a nonfluorescent tetrapeptide, Phe-Gly-Phe-Gly. First, to determine whether Phe-Gly-Phe-Gly serves as a substrate, HPLC analyses of reaction products were performed; the enzyme-dependent appearance of a product eluting at the position expected for Phe-Gly-Phe-α-hydroxy-

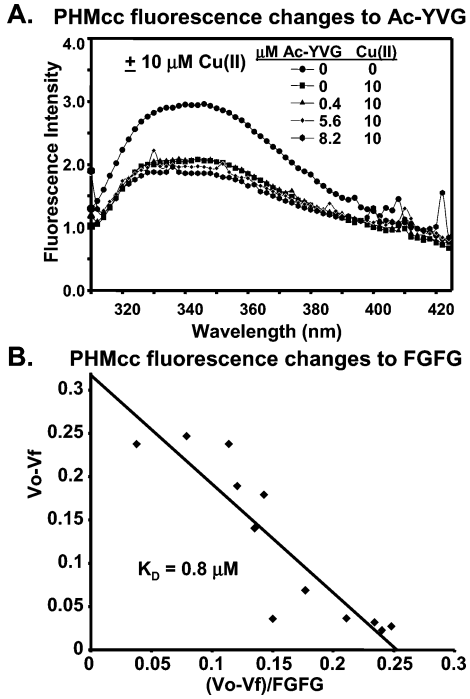

FIGURE 4: Effect of the peptidylglycine substrate on tryptophan fluorescence of purified PHMcc. (A) For the Ac-Tyr-Val-Gly substrate, Trp fluorescence does not vary with addition of the Ac-Tyr-Val-Gly peptide substrate, using 600 nM PHMcc in the presence or absence of Cu(II). Data are representative of at least three experiments of this type for PHMcc, PHMccGln^{172}Ala, and PHMccTyr^{79}Trp. (B) For the Phe-Gly-Phe-Gly (FGFG) substrate, FGFG substrate and FGF−α-hydroxylglycine product were separated on a C18 μBondapak column in 0.1% trifluoroacetic acid, and eluted with a gradient of acetonitrile, recording the absorbance at 220 nm. Addition of increasing concentrations of FGFG to PHMcc produced a graded reduction in fluorescence intensity at 344 nm; difference data are plotted as in Figure 3D, yielding a K_D of 0.8 μM for FGFG.

glycine was apparent (data not shown). The ability of the tetrapeptide to compete with ^{125}I-labeled Ac-Tyr-Val-Gly was next assessed using the wild type, PHMccGln^{170}Ala, and PHMccTyr^{79}Trp (not shown). For all three enzymes, FGFG acted as a competitive inhibitor, with a K_i value of 1−3 μM.

Knowing that Phe-Gly-Phe-Gly serves as a substrate, we evaluated the effect of this longer peptidylglycine substrate on intrinsic Trp fluorescence. A small, dose-dependent decrease in intrinsic Trp fluorescence was apparent. The increased length of Phe-Gly-Phe-Gly in comparison to Ac-Tyr-Val-Gly may account for our ability to detect its binding in this manner. Eadie−Hofstee analysis yielded a K_D for the peptidylglycine substrate of 0.8 μM for the Cu-depleted enzyme (Figure 4B). The measured K_D is in good agreement with the measured K_i (2.3 ± 0.7 μM).

Steady-State Fluorescence Spectroscopy of PHMccTyr^{79}Trp

The proximity of Tyr^{79} to Cu$_A$ raised the possibility of using Trp^{79} as an active site reporter. However, despite the presence of an additional Trp residue, PHMccTyr^{79}Trp yielded no more fluorescence intensity than PHMcc either in the absence or in the presence of copper (data not shown). Sequence analysis of PHM cDNA prepared from the PHMccTyr^{79}Trp cell line confirmed the presence of the mutation. If fluorescence from Trp^{79} is eliminated by quenching, addition of a denaturant such as guanidine HCl would be predicted to increase its fluorescence intensity. The addition of 5.45 M guanidine HCl to apoPHMcc and to apoPHMccTyr^{79}Trp shifts the λ_{max} of both proteins to 358 nm and increases their fluorescence intensity (data not shown). As predicted, after exposure to 5.45 M guanidine HCl, PHMccTyr^{79}Trp, with four Trp residues, exhibits ~30% more fluorescence intensity than an equimolar amount of PHMcc, with three Trp residues. Collectively, these results demonstrate that the 200-fold reduction in V_{max} produced by the substitution of Tyr^{79} with Trp is accompanied by the almost complete quenching of any fluorescence signal from Trp^{79}. An interaction of Trp^{79} with His^{172} might be responsible for this quenching, since neighboring Lys, Arg, and His residues are known to quench Trp fluorescence (*22*).

DISCUSSION

Intrinsic Trp fluorescence, using Trp as a reporter, provides a sensitive measure of protein tertiary structure and is widely used in protein folding studies (*22*−*24*). The high sensitivity of indole fluorescence to the polarity of the environment provides a sensitive means of monitoring the effects of metal ions and substrate on PHMcc. While EXAFS and crystallization studies are restricted by pH, solvent, and a requirement for millimolar quantities of enzyme, Trp fluorescence spectroscopy can be assessed using sub-micromolar concentrations of metal-free or fully metalated enzyme. Dissociation constants (K_D) can be determined under a wide range of conditions. In the presence or absence of copper, the emission intensity maximum (λ_{max}) of the wild type, PHMccGln^{170}Ala, and PHMccTyr^{79}Trp was 344 nm, indicating that the detectable tryptophan residues are only partially solvent exposed (*22*). The signal from the additional Trp residue in PHMccTyr^{79}Trp was totally quenched.

The changes in intrinsic Trp fluorescence observed upon addition of copper to PHMcc allowed us to draw two conclusions. First, the conformation of PHMcc is altered upon binding copper. Second, copper binds with a K_D of 0.06 μM, nearly identical to the K_D predicted (0.1 μM) by computer simulation of the copper-dependent activation of PAM (*13*). Consistent with this value, PHMcc has maximal enzyme activity when assayed in the presence of 0.5 μM copper (*16*). Higher concentrations of copper both inhibit activity (K_I = 25 μM) (*13*) and further quench fluorescence (Figure 3). Many cytosolic cuproproteins bind copper far more avidly (*25*), raising interesting questions about how PHM retains the copper it needs for activity.

With Phe-Gly-Phe-Gly as a substrate, we were able to use changes in Trp fluorescence to determine a K_D of 0.8 μM. The Michaelis constant (K_m) for Phe-Gly-Phe-Gly could not be precisely determined, due to limitations in sensitivity during HPLC, but is clearly below 3 μM. The K_i determined for Phe-Gly-Phe-Gly competing with [^{125}I]-*N*-acetyl-Tyr-Val-Gly is similar, 2.4 μM. Knowing that the Michaelis constant (K_m) is similar to the actual binding constant of the peptidylglycine substrate (K_D) argues that the rate-limiting step in the multisubstrate reaction is downstream of the binding of peptidylglycine to PHM, and that the peptide−PHM complex is effectively equilibrated (*20*, *21*, *26*). The fact that the K_i for Phe-Gly-Phe-Gly is lower than the K_i for Ac-Tyr-Val-Gly (*16*) presumably reflects additional substrate−

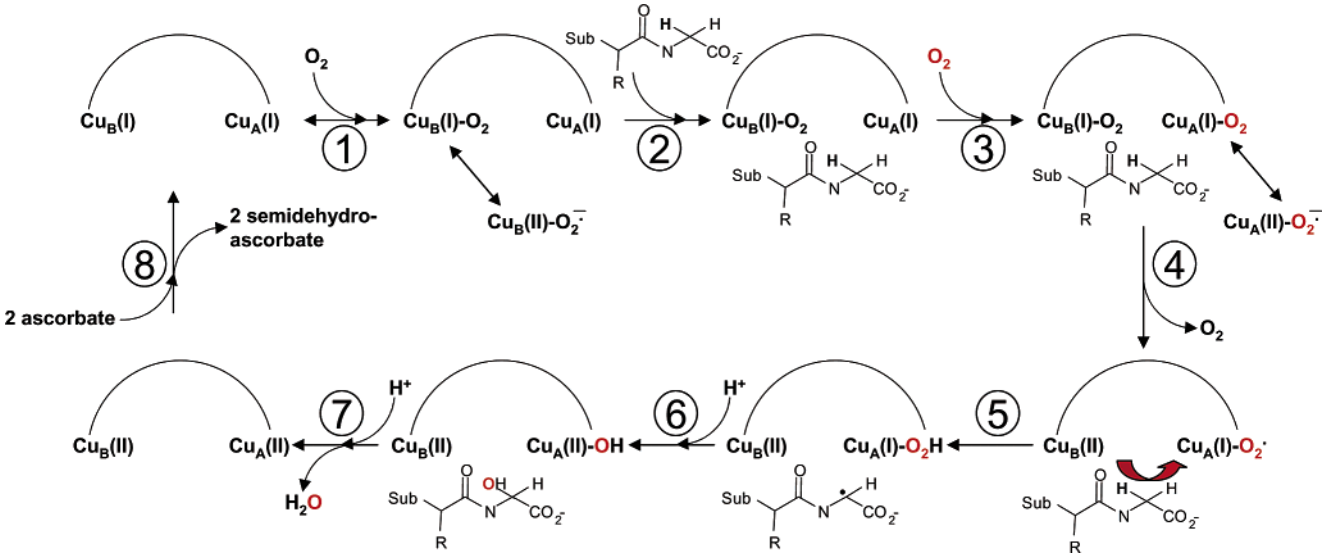

FIGURE 5: Proposed mechanism for PHMcc-catalyzed α-hydroxylation of peptidylglycine substrates. Dioxygen binds to reduced copper at the Cu_B site, equilibrating with the $Cu_B(II)-$superoxide resonance form. Peptidylglycine binding induces the binding of dioxygen at the Cu_A site. An electron transfer pathway that includes dioxygen bound to Cu_B, substrate, and dioxygen bound to Cu_A allows formation of the $Cu_A(I)-$superoxide species, with release of dioxygen from $Cu_B(II)$. To position the *pro-S* hydrogen from the α-carbon of glycine for abstraction, the peptidylglycine substrate must either swivel from its crystallographically defined site or bind at an additional site. The remainder of the reaction could then proceed through the steps outlined by Prigge et al. (*15*), with the substrate radical attacking hydroperoxide bound to Cu_A.

protein backbone interactions and is consistent with earlier kinetic measurements (*27*). This type of interaction is absent from α-*N*-acetyl-3,5-diiodo-Tyr-Gly, the only substrate examined crystallographically.

The effects of pH on PHM are striking, with V_{max} decreasing ~25-fold from pH 5.5 (intragranular pH) to pH 7.0 (cytosolic pH) (Table 1). Although crystallographic studies of PHM were conducted at pH 5.5 (*15*), EXAFS and carbon monooxide binding studies were conducted at pH 7.5 (*6*), perhaps explaining some of the apparent discrepancies. The proposed role for protonation of His^{172} would be consistent with the observed decrease in V_{max} at pH 7 (*28*). The existence of an active site base near Cu_A suggests that important reaction chemistry occurs at this site. The fact that the K_m for *N*-acetyl-Tyr-Val-Gly decreases with increasing pH may reflect an increased affinity of the deprotonated Gly carboxylate for Arg^{240}. Tighter binding of the substrate to Arg^{240} may lock the substrate in a position that is incompatible with hydrogen atom abstraction. A potent mechanism-based inhibitor of PHM, 4-phenyl-3-butenoic acid, also serves as a substrate (*29*); multiple products are generated, and their identity suggests a role for a delocalized free radical as well as movement of substrate within the catalytic site.

On the basis of a detailed analysis of kinetic isotope effects, PHM and DBM employ very similar reaction mechanisms, with similar transition-state structures (*30*). Therefore, data from both enzymes can be employed to propose a unifying reaction mechanism. Two ascorbate-mediated single-electron reductions occur before substrate binds. In the secretory granule environment, with its high levels of reduced ascorbate (*4*), the reaction cycle starts with both Cu_A and Cu_B reduced (Figure 5). While *N*-benzoylglycine (hippuric acid) exhibits equilibrium ordered kinetics, larger peptides exhibit steady-state ordered kinetics (*30*). The molecular oxygen consumed in the reaction binds only to the E·S complex, perhaps as a result of subtle substrate-induced conformational changes, as suggested by our fluorescence studies. Discrepancies in the predicted transition-state structures, based on primary and secondary isotope effects, along with the magnitude of the primary isotope effect, suggest the occurrence of tunneling and coupled motion as PHM activates the C−H bond of its peptidylglycine substrate (*30*, *31*).

One of the most striking features of the reactions catalyzed by PHM and by DBM is the stability of the reduced enzyme in the presence of molecular oxygen and in the absence of substrate (*11*, *32*−*34*). Potentially toxic reactive oxygen species are not generated at any significant rate, an important feature for any monooxygenase. In the absence of substrate, molecular oxygen binds to Cu_B, which has features common to electron transfer sites in other cuproproteins (*6*, *8*, *19*). In the presence of substrate, studies of carbon monooxide binding suggest that molecular oxygen also binds to Cu_A (*6*). Mechanistically, substrate-induced binding of molecular oxygen is critical. Cu_A has features common to oxygen binding sites in cuproproteins that function in redox reactions and oxygen transport (*19*). The fact that peptide binding activates CO reactivity at Cu_A, with the CO stretching frequency dependent on the substrate bound (*6*), suggests that the oxygen that is cleaved during substrate hydroxylation binds at this site.

The fundamental problem in understanding the reaction catalyzed by PHM is how the single reducing equivalents transferred from two ascorbic acid residues to Cu_A and Cu_B, which are more than 10 Å apart, participate together in the reaction. The two domains of PHM interact through a large hydrophobic interface formed by residues that are highly conserved across species; more than 500 $Å^2$ of both domains is buried, with further stabilization by hydrogen-bonded antiparallel β-sheets linking the two domains (*19*). Both crystallographic and spectroscopic data indicate that Cu_A and Cu_B remain separated during the reaction cycle (*7*, *15*, *19*). Crystallographic data led us to propose a substrate-mediated electron transfer pathway in which Gln^{170} played a critical

role linking His^{108} to a water bound to the carboxylate of the peptide substrate (*15*). Given that replacement of Gln^{170} with a smaller residue like Ala or Asn has no effect on K_m or V_{max}, Gln^{170} cannot play the role proposed in the original substrate-mediated electron transfer pathway. Crystallographic studies of reduced PHMcc in which Gln^{170} has been replaced with Ala should reveal any alternate electron transfer pathway. Replacement of Gln^{170} with a residue of a similar size (Glu or Leu) decreased V_{max} 20-fold, suggesting that these larger residues interfere with the normal reaction pathway.

In addition to all of the Cu ligands, residues whose mutation substantially diminishes V_{max} include Tyr^{79} (200-fold decrease for Trp^{79}), Gln^{170} (20-fold decrease for Leu^{170}), Arg^{240} (200-fold decrease for Gln^{240}), and Glu^{313} (6-fold decrease for Asp^{313}) (*16*, *19*) (Figure 1C). Residues whose mutation primarily decreases the affinity for acetyl-Tyr-Val-Gly include Tyr^{318} (8-fold decrease for Phe^{318}), Met^{314}, and Glu^{313} (8-fold decrease for Asp^{313}) (*16*). Despite the proximity of the glycyl carboxylate to Arg^{240}, K_m is scarcely altered by mutation to Gln^{240}. The crystallographically defined substrate binding site is intimately connected to Cu_B, and redox-mediated changes in Cu_B would be expected to affect this interaction (*14*). Two Cu_B ligands, His^{242} and His^{244}, follow Arg^{240} in β-strand 14. Met^{314}, Asn^{316}, and Phe^{318}, situated in β-strand 21, each interact with the substrate. Redox sensitive movement of Met^{314} toward Cu_B would be accompanied by a change in the substrate binding site. Glu^{313} makes a hydrogen bond with His^{242}, anchoring the Met^{314} loop to the His^{242} loop at the Cu_B site (*14*). Lacking any evidence for a second substrate binding site near Cu_A, we suggest that a change in the orientation of the Cu_B ligands is transformed into a change in the substrate binding site, allowing the peptidylglycine substrate to move toward Cu_A. This movement would allow the peptidylglycine substrate to form part of the electron transfer pathway between Cu_A and Cu_B.

Taking into account the available data, we suggest that molecular oxygen binds to the Cu_B site of reduced PHM, with an equilibrium between the $Cu(I)-O_2$ and $Cu(II)-$superoxide species (Figure 5, step 1). Binding of peptidylglycine substrate, through its extensive interactions with Met^{314}, Asn^{316}, and Tyr^{318} on β-strand 21 (Figure 1C), alters the structure of the active site, facilitating the binding of molecular oxygen to Cu_A in addition to Cu_B and moving toward Cu_B (steps 2 and 3) (*6*, *8*). Both His^{172}, a Cu_A ligand and potential active site base (*28*), and Gln^{170} are redox sensitive, with His^{172} moving closer to Cu_A and Gln^{170} losing a hydrogen bond to His^{108} upon oxidation (*15*). Although small residues can replace Gln^{170} with no decrease in activity, larger residues cannot, presumably because they interfere with changes that occur in the active site. In conjunction with the reoriented peptidylglycine substrate, molecular oxygens bound simultaneously to Cu_A and Cu_B make it possible to span the gap. Using this pathway, Cu_B donates its reducing equivalent to the $Cu(II)_A-$superoxide resonance form, allowing dioxygen to dissociate from $Cu_B(II)$ (step 4). Reversing the roles of Cu_A and Cu_B, the mechanism proposed previously is applicable (*15*). The reduced $Cu(I)_A-$superoxide species is responsible for the chemistry of the reaction, abstracting hydrogen, forming a peptide glycyl radical, and generating the $Cu_A(I)-$hydroperoxide species (step 5). This role for Cu_A supported its ligand-dependent binding of molecular oxygen, its proximity to His^{172}, the sensitivity of V_{max} to pH, and the total quenching of the fluorescence signal from Trp^{79}, coupled with the 200-fold reduction in the V_{max} of $PHMccTrp^{79}$. Heterolytic cleavage of the oxygen bound at Cu_A occurs following attack by the glycyl radical, with reduction and protonation of the oxygen bound to Cu_A, perhaps involving His^{172} (step 6), followed by dissociation through protonation (step 7). Reduction of both Cu_A and Cu_B occurs quickly in the presence of the millimolar levels of reduced ascorbate in secretory granules (step 8). By taking into account the substrate-dependent nature of oxygen consumption by these copper-dependent monooxygenases, we are able to propose a testable mechanism that does not rely on the need for electrons or superoxide to move long distances through the solvent or peptide backbone.

ACKNOWLEDGMENT

We thank Jianping Huang for her help in producing recombinant protein, Tracey Hand for her help with mutagenesis, and Yanping Wang for her help analyzing cDNAs.

REFERENCES

1. Blain, I., Slama, P., Giorgi, M., Tron, T., and Reglier, M. (2002) *J. Biotechnol. 90*, 95−112.
2. Decker, H., and Terwilliger, N. (2000) *J. Exp. Biol. 203*, 1777−1782.
3. McGuirl, M. A., and Dooley, D. M. (1999) *Curr. Opin. Chem. Biol. 3*, 138−144.
4. Prigge, S. T., Mains, R. E., Eipper, B. A., and Amzel, L. M. (2000) *Cell. Mol. Life Sci. 57*, 1236−1259.
5. Garcia-Borron, J. C., and Solano, F. (2002) *Pigm. Cell Res. 15*, 162−173.
6. Jaron, S., and Blackburn, N. J. (1999) *Biochemistry 38*, 15086−15096.
7. Boswell, J. S., Reedy, B. J., Kulathila, R., Merkler, D. J., and Blackburn, N. J. (1996) *Biochemistry 35*, 12241−12250.
8. Jaron, S., and Blackburn, N. J. (2001) *Biochemistry 40*, 6867−6875.
9. Reedy, B. J., and Blackburn, N. J. (1994) *J. Am. Chem. Soc. 116*, 1924−1931.
10. Eipper, B. A., Quon, A. S. W., Mains, R. E., Boswell, J. S., and Blackburn, N. J. (1995) *Biochemistry 34*, 2857−2865.
11. Freeman, J. C., Villafranca, J. J., and Merkler, D. J. (1993) *J. Am. Chem. Soc. 115*, 4923−4924.
12. Kulathila, R., Merkler, K. A., and Merkler, D. J. (1999) *Nat. Prod. Rep. 16*, 145−154.
13. Kulathila, R., Consalvo, A. P., Fitzpatrick, P. F., Freeman, J. C., Snyder, L. M., Villafranca, J. J., and Merkler, D. J. (1994) *Arch. Biochem. Biophys. 311*, 191−195.
14. Blackburn, N. J., Rhames, F. C., Ralle, M., and Jaron, S. (2000) *JBIC, J. Biol. Inorg. Chem. 5*, 341−353.
15. Prigge, S. T., Kolhekar, A. S., Eipper, B. A., Mains, R. E., and Amzel, L. M. (1999) *Nat. Struct. Biol. 6*, 976−983.
16. Kolhekar, A. S., Keutmann, H. T., Mains, R. E., Quon, A. S. W., and Eipper, B. A. (1997) *Biochemistry 36*, 10901−10909.
17. Kolhekar, A. S., Bell, J., Shiozaki, E. N., Jin, L., Keutmann, H. T., Hand, T. A., Mains, R. E., and Eipper, B. A. (2002) *Biochemistry 41*, 12384−12394.
18. Bell-Parikh, L. C., Eipper, B. A., and Mains, R. E. (2001) *J. Biol. Chem. 276*, 29854−29863.
19. Prigge, S. T., Kolhekar, A. S., Eipper, B. A., Mains, R. E., and Amzel, L. M. (1997) *Science 278*, 1300−1305.
20. Fersht, A. (1985) *Enzyme structure and mechanism*, W. H. Freeman and Co., New York.
21. Segel, I. H. (1975) *Enzyme kinetics: behavior and analysis of rapid equilibrium and steady-state enzyme systems*, John Wiley and Sons, New York.
22. Lakowicz, J. R. (1999) *Principles of fluorescence spectroscopy*, Kluwer Academic/Plenum, Boston.

23. Clayton, A. H., and Sawyer, W. H. (2002) *Eur. Biophys. J. 31*, 9−13.
24. Cioni, P., and Strambini, G. B. (2002) *Biochim. Biophys. Acta 1595*, 116−130.
25. O'Halloran, T. V., and Culotta, V. C. (2000) *J. Biol. Chem. 275*, 25057−25060.
26. Walsh, C. (1979) *Enzymatic Reaction Mechanisms*, W. H. Freeman and Co., San Francisco.
27. Tamburini, P. P., Jones, B. N., Consalvo, A. P., Young, S. D., Lovato, S. J., Gilligan, J. P., Wennogle, L. P., Erion, M., and Jeng, A. Y. (1988) *Arch. Biochem. Biophys. 267*, 623−631.
28. Jaron, S., Mains, R. E., Eipper, B. A., and Blackburn, N. J. (2002) *Biochemistry 41*, 13274−13282.
29. Driscoll, W. J., Konig, S., Fales, H. M., Pannell, L. K., Eipper, B. A., and Mueller, G. P. (2000) *Biochemistry 39*, 8007−8016.
30. Francisco, W. A., Merkler, D. J., Blackburn, N. J., and Klinman, J. P. (1998) *Biochemistry 37*, 8244−8252.
31. Francisco, W. A., Knapp, M. J., Blackburn, N. J., and Klinman, J. P. (2002) *J. Am. Chem. Soc. 124*, 8194−8195.
32. Brenner, M. C., and Klinman, J. P. (1989) *Biochemistry 28*, 4664−4670.
33. Kaufman, S. (1974) *J. Psychiatr. Res. 11*, 303−316.
34. Friedman, S., and Kaufman, S. (1965) *J. Biol. Chem. 240*, 4763−4773.

BI034247V